Dynamics for a two-dimensional antisymmetric map

1994 J. Phys. A: Math. Gen. 27 5187

(http://iopscience.iop.org/0305-4470/27/15/018)

J. Phys. A: Math. Gen. 27 (1994) 5187–5200. Printed in the UK

Dynamics for a two-dimensional antisymmetric map

H-P Fang

CCAST (World Laboratory) PO Box 8730, Beijing, 100080, People's Republic of China
and
Institute of Theoretical Physics, PO Box 2735, Beijing, 100080, People's Republic of China†

Received 19 February 1994, in final form 13 June 1994

Abstract. A two-dimensional representation of symbolic dynamics for a two-dimensional map with antisymmetric property is constructed. The behaviour of symmetry-breaking periodic orbits, symmetry-breaking bifurcations, symmetry-breaking attractors and the boundaries of basins between co-existing attractors are then discussed using this representation of symbolic dynamics.

1. Introduction

Since the discovery of the chaotic attractor introduced by E N Lorenz [1], chaos has become an important concept in nearly all branches of natural sciences. The differential equations, which are believed to govern our natural world and may exhibit chaotic attractors, are widely discussed. Among these differential equations, the Lorenz equations itself, the double-diffusive convection system [2] which originates from convections in the atmosphere and in the ocean (binary mixture) and the Duffing equations [3] which describes the damped, periodically forced nonlinear oscillator have received considerable attention. All of these systems possess a discrete symmetry. Subsequently, the orbits for these ODEs are partitioned into two classes, the symmetric orbits and the asymmetric orbits, according to their retaining or not retaining the symmetry. It has been shown that a symmetric periodic orbit will first undergo symmetry-breaking bifurcation to a pair of asymmetric orbits of the same period as the original one, then enjoy period-doubling bifurcations [4].

A study of these ODEs is greatly facilitated by the construction and study of their Poincaré mappings on proper Poincaré sections. Take, for example, the Lorenz equations

$$\begin{aligned} \dot{x} &= \sigma(y - x) \\ \dot{y} &= rx - xz - y \\ \dot{z} &= xy - bz. \end{aligned} \tag{1}$$

In these equations, σ =10, b = 8/3 and r is the controlling parameter. The Poincaré section $z = r - 1$ is widely used and the attractors on this plane are called the Lorenz attractors. Figure 1(a, b) shows the Poincaré mapping and the first return map for $r = 140$. Figure 1(b) is obtained by plotting the successive x_{n+1} versus x_n in the plane $z = r - 1$. This figure displays a sketch of a one-dimensional (1D) map with two critical points and the antisymmetric property (figure 2)

$$x_{n+1} = Ax_n^3 + (1 - A)x_n \tag{2}$$

† Mailing address.

0305-4470/94/155187+14$19.50

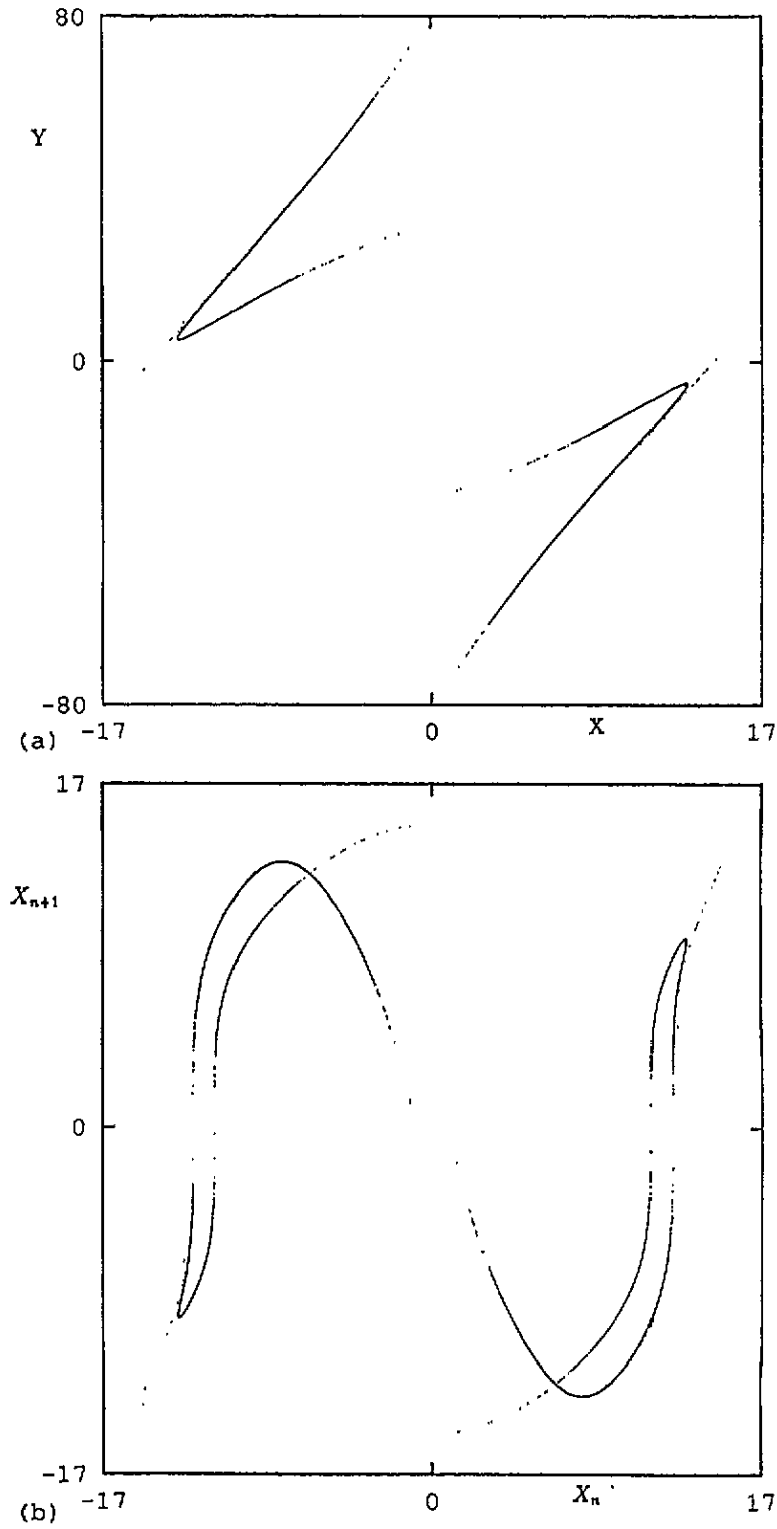

Figure 1. The Poincaré mapping (*a*) and the first return map (*b*) for $r = 140$ for the Lorenz equations in the plane $z = r - 1$.

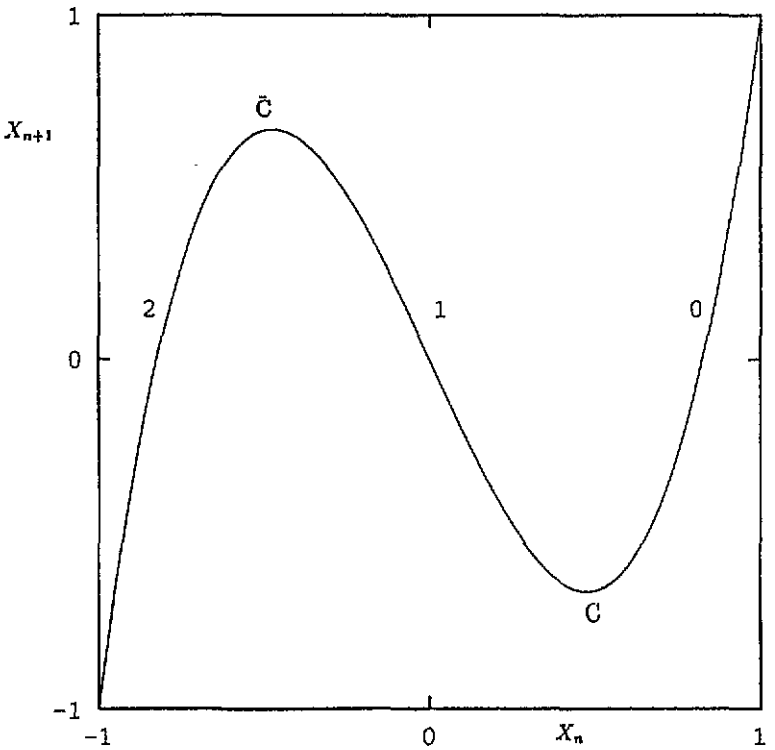

Figure 2. The shape of the one-dimensional antisymmetric map $x_{n+1} = Ax_n^3 + (1 - A)x_n$. $\bar{C}$ and C denote two critical points which divide the interval $[-1, 1]$ into three monotonic segments marked by 0, 1 and 2.

where parameter A varies in $[1, 4]$. Similar behaviour is also observed for many ODEs with antisymmetric property [2, 3]. Obviously, the attractors for the logistic map or the Hénon map [5], which do not share the antisymmetric property, are qualitatively different from the first return maps and the Poincaré mappings for these ODEs. In fact, it has already been found that the periodic windows, interspersed in chaotic regions for these ODEs with antisymmetric property, can be approximately ordered as those of the 1D maps with two critical points and antisymmetric property (see equation (2)). For the Lorenz equations, from $r = 50$ up to $r = 400$, 53 stable periodic windows are found numerically (the period-doubling regimes did not count), among which 47 can fit into the stable periodic windows for map (2) [6, 7].

Despite these observations, it is clear from the first return map shown in figure 1(*b*) that a 1D map cannot reveal the complex topology of the attractors for these ODEs. In order to determine the characteristic properties of these attractors, it is necessary to discuss the behaviour of two-dimensional (2) attractors on proper Poincaré sections of these ODEs directly. For the complexity of chaotic dynamics of the ODEs, as that had been proposed by M Hénon [5], we will consider in this paper a 2D map extended from the 1D map (2) as follows:

$$\begin{pmatrix} x_{n+1} \\ y_{n+1} \end{pmatrix} = F(x_n, y_n) = \begin{pmatrix} Ax_n^3 + (1 - A)x_n + by_n \\ x_n \end{pmatrix}. \tag{3}$$

This map is also invariant under the transformation

$$x \to -x \qquad y \to -y. \tag{4}$$

We expected that some behaviour of the 2D attractors for these ODEs with antisymmetric property, such as the Lorenz equations and the Duffing equations, can be approached by this map.

To study the chaotic dynamics of dynamical systems, it is widely accepted that a most useful way is to consider the set of unstable periodic orbits embedded in them [8–13]. It was shown that characteristic quantities of strange attractors like Lyapunov exponents, entropies, dimensions and $f(\alpha)$ spectra can be directly related to properties of unstable periodic orbits. Until recently symbolic dynamics provided the most robust technique for the calculation and classification of unstable periodic orbits in dynamical systems [6–12].

In this paper, we first construct a two-dimensional representation of symbolic dynamics for this 2D map. Then we discuss the dynamics for this map, especially that related to the symmetry (4).

The paper is organized as follows. In section 2, the symbolic dynamics for the map (3) is constructed and its validity is checked. Unlike that of the Hénon map, a ternary partition is convenient for this map. It has been well known that a symmetrical periodic orbit cannot undergo period-doubling bifurcation in co-dimension-one systems [4]. In section 3, the case for this system with two parameters is considered using symbolic dynamics. In section 4, the topology for the symmetry-breaking attractors of the map (3) is discussed. It is found that the chaotic dynamics for these symmetry-breaking attractors is close to 1D and can be approximately treated as that of 1D map to some degree. In section 5, a geometric description of the symbolic dynamics is presented and basin boundaries between coexisting attractors are understood in terms of this geometric description. Finally, our conclusions are given in section 6.

2. Construction of symbolic dynamics for the 2D antisymmetric map (3)

To construct the symbolic dynamics of a dynamical system, the determination of the partition and the ordering rules for the underlying symbolic sequences is of crucial importance. In the case of 1D mappings, the partition is composed of all the critical points. For example, for the antisymmetric cubic map (2), a ternary partition marked by $\bar{C}$ and C divide the interval $[-1, 1]$ into three monotonic branches (figure 2). The right branch to C is assigned 0, the left branch to $\bar{C}$ is assigned 2, whereas the part between $\bar{C}$ and C is 1. As a consequence, nearly all trajectories are unambiguously encoded by infinite strings of bits $S(x) = (s_1 s_2 \cdots)$ where s_i is either 0, 1 or 2 [6]. Referring to the natural ordering of the real numbers in the 1D interval $[-1, 1]$, the ordering rules for these symbolic strings can be defined, that is, considering two symbolic strings $S(x_1)$ and $S(x_2)$ from the initial points x_1 and x_2, $S(x_1) \geqslant S(x_2)$ if and only if $x_1 > x_2$. Analytically, these ordering rules correspond to the natural orderings for the 'forward' variables

$$\alpha(S(x)) = \sum_{i=1}^{\infty} \mu_i 3^{-i} \tag{5}$$

with

$$\mu_i = \begin{cases} 0 \\ 1 \\ 2 \end{cases} \quad \text{for} \quad \begin{cases} s_i = 2 \\ s_i = 1 \ \text{ and } \ \sum_{j=1}^{i} s_i = 0 \ (\text{mod } 2) \\ s_i = 0 \end{cases}$$

$$\text{or} \quad \begin{cases} s_i = 0 \\ s_i = 1 \\ s_i = 2 \end{cases} \text{and} \sum_{j=1}^{i} s_i = 1 \pmod 2.$$

Once the kneading sequence K_g and K_s (i.e. the forward symbolic sequences from the maximal and minimal values $\bar{C}$ and C) are determined and $\alpha(K_g)$, $\alpha(K_s)$ are calculated, the grammar for a word allowed or forbidden is obtained, which is: A word $S(x)$ corresponds to a real trajectory if and only if it satisfies

$$\alpha(K_s) \leqslant \alpha(\sigma^m(S(x))) \leqslant \alpha(K_g) \qquad m = 0, 1, 2, \cdots \tag{6}$$

where σ denotes the shift operator. Consequently, the characteristic quantities of strange attractors of map (2) for given parameters are completely determined.

For 2D maps, if one wants to split the full phase space into parts, 1D curves should be introduced, known as partition lines. For the Hénon map, it has been verified that a binary generating partition is convenient, which is the set of all 'primary' tangencies between stable and unstable manifolds [9]. For the 2D map (3) extended from the 1D antisymmetric cubic map, all 'primary' tangencies between stable and unstable manifolds form a ternary generating partition $\bar{C}$ and C. $\bar{C}$ and C is symmetric to (0,0) from the antisymmetric property of this 2D map. In figure 3, the partition (dashed lines) together with the strange attractor for $(A, b) = (3.4, 0.25)$ is shown. By analogy to those of the 1D map (2), the letters 0, 1 and 2 are assigned to different parts. For this 2D map, x_i depends not only on x_{i-1},

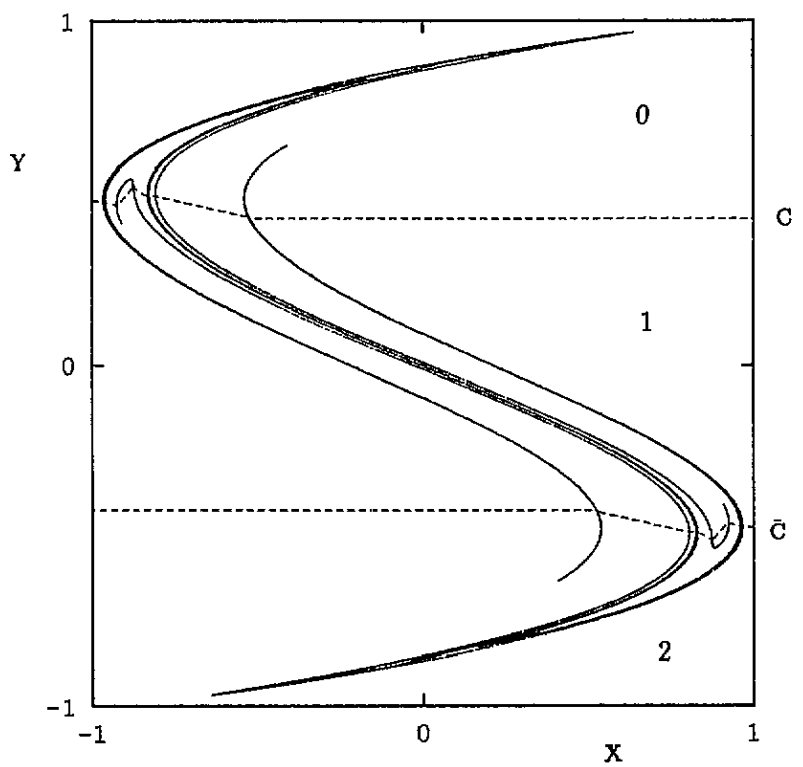

Figure 3. The attractor and the ternary partition for the 2D antisymmetric cubic map for $(A, b) = (3.4, 0.25)$. The dashed lines are partition C and $\bar{C}$ by connecting the 'primary' tangent points between stable and unstable manifolds. The ternary partition splits the phase space into three parts as we expected.

but also on x_{i-2}, so that backward sequences have to be considered. All trajectories are then encoded by double-infinite strings of bits $S(x, y) = \cdots s_{-m} \cdots s_{-2}s_{-1}s_0 \bullet s_1 s_2 \cdots s_n \cdots$, where s_0 denotes the letter for the initial point (x, y), s_n denotes the letter for the nth image, s_{-m} the letter for the mth pre-image (each assuming the values 0, 1 or 2), and the solid dot indicates the 'present' position. Hereafter we call the part $\bullet s_1 s_2 \cdots s_n \cdots$ the forward word from (x, y), and the part $\cdots s_{-m} \cdots s_{-2}s_{-1}s_0\bullet$ the backward word; they are represented by Forw$(S(x, y))$ and Back$(S(x, y))$, respectively. Subsequently, the 'forward' variables defined in equation (5) are

$$\alpha(S(x, y)) = \alpha(\text{Forw}(S(x, y))).$$

In order to extend the grammar for the 1D cubic map (2) to the 2D map (3), we introduce 'backward' variables defined as

$$\beta(S(x, y)) = \beta(\text{Back}(S(x, y)) = \sum_{i=0}^{\infty} \nu_i 3^{-(i+1)} \tag{7}$$

with

$$\nu_i = \begin{cases} 0 \\ 1 \\ 2 \end{cases} \quad \text{for} \quad \begin{cases} s_{-i} = 2 \\ s_{-i} = 1 \\ s_{-i} = 0 \end{cases} \quad \text{and} \quad \sum_{j=0}^{i-i}(1 - s_j) = 0 \pmod 2$$

$$\text{or} \quad \begin{cases} s_{-i} = 0 \\ s_{-i} = 1 \\ s_{-i} = 2 \end{cases} \quad \text{and} \quad \sum_{j=0}^{i-i}(1 - s_j) = 1 \pmod 2.$$

The space spanned by α and β is called the symbolic plane. Each symbolic sequence $S(x, y)$ corresponds to a point $(\alpha(S(x, y)), \beta(S(x, y)))$ in this symbolic plane (we will hearafter simply call it the point $S(x, y)$).

As those in the Hénon map, where all topological properties can be retrieved from the kneading sequences (the symbolic sequences from the partition), we determine the grammar of this 2D antisymmetric map as follows. From the antisymmetric property of the map (3), only the points on $\bar{C}$ need be considered to construct the pruning fronts. To each primary tangency P on $\bar{C}$ with a double-infinite kneading sequence $K = \cdots s_{-m} \cdots s_{-2}s_{-1}s_0 \bullet s_1 s_2 \cdots s_n \cdots$ (with s_0, which may be 1 or 2, undetermined), a forward variable $\alpha(K)$ associates with two symmetrical backward variables $\beta_-(K) = \beta(\cdots s_{-m} \cdots s_{-1}2\bullet)$ and $\beta_+(K) = \beta(\cdots s_{-m} \cdots s_{-1}1\bullet) = 2/3 - \beta_-(K)$. Analogously to those in the Hénon map [10], for all allowed points (α, β) with $\beta \in [\beta_-(K), \beta_+(K)]$, α should be less than $\alpha(K)$ and thus one pruning front is obtained by cutting out rectangles $\{\alpha, \beta | \alpha > \alpha(K), \beta \in [\beta_-(K), \beta_+(K)]\}$ for all P. It is clear that all the points right to this pruning front are not allowed. We call the set of all these points a fundmental forbidden zone (FFZ). From the antisymmetric property, the other pruning front and FFZ are symmetrical to above fronts with respect to the centre $(1/2, 1/2)$ of the symbol plane. Figure 4 shows the symbolic plane for $(A, b) = (3.4, 0.25)$ in which the pruning fronts are constructed with 62 points on $\bar{C}$. It is clear that the pruning front is monotonic in the sub-plane with $\beta < 1/3$.

To check the above grammar, we select 60 000 points randomly on the attractor for $(A, b) = (3.4, 0.25)$, calculate the (α, β) values for these points which are also shown in figure 4. No points are contained in the FFZs although many points are very close to the pruning fronts.

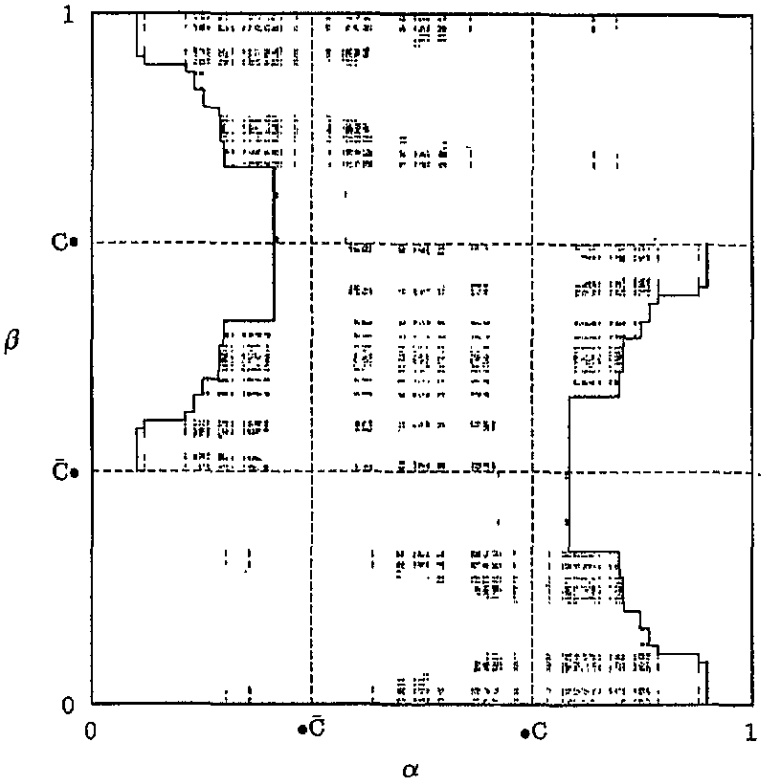

Figure 4. Points representing real orbits generated from the 2D antisymmetric cubic map for $(A, b) = (3.4, 0.25)$ are shown together with the pruning fronts in the symbolic plane.

From this grammar we can estimate all the admissible words. In table 1, we list all the 'primitive' admissible words up to period eight for $(A, b) = (3.4, 0.25)$. The 'primitive' words cannot be repetitions of lower cycles.

The validity of the above grammar can be checked directly by comparing the unstable periodic orbits from this grammar and those by the Newton–Raphson technique. In practice we record a period-n orbit if the change of position after the nth iteration is smaller than a test

Table 1. All the allowed 'primitive' periodic orbits up to period 8. The letter X stands for 1 or 2. Only non-repeating strings of the sequences are presented. And the conjugate words are not listed.

Period	*Allowed Sequence*	*Period*	*Allowed Sequence*
1	X	7	011120X
2	0X	8	0020110X
4	0102	8	01020101
5	0110X	8	0111010X
6	01020X	8	0112010X
6	01110X	8	0102020X
6	01120X	8	0111020X
7	011010X	8	0111110X
7	011020X	8	0111120X
7	011110X	8	0112020X

value $\epsilon = 10^{-9}$. We check the symbolic sequences for these periodic orbits one by one up to a period 9. The results agree exactly with those predicted by the above grammar. However, this technique can be applied only to short unstable cycles, since chaotic attractors exhibit sensitivity to initial conditions and numerical errors grow exponentially with the length of the cycle. Recently, another method was developed to check the availability of the grammar for the map with a binary partition [8]. An extended approach for the map (3) with a ternary partition is applied.

Once the ordering rules and the grammar for a word allowed or forbidden are determined, the symbolic dynamics for this 2D map is constructed. In what follows we discuss the topological property of this map with this symbolic dynamics. We focus on the behaviour of symmetry-breaking periodic orbits, symmetry-breaking bifurcations and symmetry-breaking attractors. At last we give a geometric description of the symbolic dynamics and discuss the basin boundaries between coexisting attractors.

3. The symmetry-breaking periodic orbits and symmetry-breaking bifurcations

It is well known that systems with symmetric property are typically associated with spontaneous symmetry breaking. For map (3), a symmetric periodic orbit satisfies

$$F^{(n/2)}(x, y) = -\begin{pmatrix} x \\ y \end{pmatrix}$$

n being the period of the orbit and (x, y) being an element on the orbit, and asymmetric orbits do not satisfy this relation. Symbolically, a symmetric orbit $S(x, y)$ will be one of the following forms

$$(\Sigma 0 \bar{\Sigma} 2)^{\infty} \tag{8}$$

$$(\Sigma 1 \bar{\Sigma} 1)^{\infty} \tag{9}$$

where Σ is a substring of letters 0, 1 and 2 and $\bar{\Sigma}$ is the conjugate of Σ obtained by interchanging 0's and 2's but leaving 1's unchanged. Hereafter we omit the repeating strings of the periodic sequences and simply denote them by $\Sigma 0 \bar{\Sigma} 2$ and $\Sigma 1 \bar{\Sigma} 1$. An asymmetric cycle cannot be written in any of these forms.

For the convenience of the discussion that follows, we always let

$$\alpha(\sigma^m(\mathrm{S}(x, y))) \leqslant \alpha(\mathrm{S}(x, y)) \qquad m = 0, \pm 1, \pm 2, \cdots \tag{10}$$

where σ denotes the shift operator. Forw$(S(x, y))$ is maximal in all the shifts of $S(x, y)$. Numerically, it has been found that once a symmetry-breaking orbit is admissible, its antisymmetric and symmetric counterparts are allowed. We list some of them with period 10 in table 2 for $(A, b) = (3.4, 0.25)$.

This can be partly understood from the symbolic dynamics constructed in section 2. Without losing generality, we assume that there exists a symmetry-breaking orbit $\Sigma 0 \bar{\Sigma} 1$.

Table 2. Some symmetrical and symmetry-breaking periodic orbits

Period	Symmetrical words	Asymmetrical words	Asymmetrical words
10	0112121101	0112121102	2110101120
10	0112021102	0112021101	2110201121
10	0102021202	0102021201	2120201021
10	0102121201	0102121202	2120101020

From the antisymmetric property of the pruning fronts, the antisymmetric word $\Sigma 1\bar{\Sigma}2$ exists. The symmetric counterpart of $\Sigma 0\bar{\Sigma}1$ is $\Sigma 0\bar{\Sigma}2$. From equations (5) and (7), we have

$$\begin{aligned} &\alpha(\bullet(\Sigma 0\bar{\Sigma}2)^{\infty}) < \alpha(\bullet(\Sigma 0\bar{\Sigma}1)^{\infty}) \\ &\beta((\Sigma 0\bar{\Sigma}2)^{\infty}\bullet) < \beta((\Sigma 0\bar{\Sigma}1)^{\infty}\Sigma 0\bar{\Sigma}2\bullet). \end{aligned} \tag{11}$$

Point $(\Sigma 0\bar{\Sigma}2)^{\infty} \bullet (\Sigma 0\bar{\Sigma}2)^{\infty}$ is down-left to the point $(\Sigma 0\bar{\Sigma}1)^{\infty}\Sigma 0\bar{\Sigma}2 \bullet (\Sigma 0\bar{\Sigma}1)^{\infty}$ in the symbolic plane.

In the symbolic plane, $1/3-\beta((\Sigma 0\bar{\Sigma}2)^{\infty}\bullet)$ is the distance between the word $(\Sigma 0\bar{\Sigma}2)^{\infty}$ and partition $\bar{C}\bullet$, whereas $1/3-\beta((\Sigma 0\bar{\Sigma}1)^{\infty}\Sigma 0\bar{\Sigma}2\bullet)$ is the distance between the word $(\Sigma 0\bar{\Sigma}1)^{\infty}$ and partition $\bar{C}\bullet$. From the monotonic property of the pruning front in the sub-plane with $\beta < 1/3$, point $(\Sigma 0\bar{\Sigma}2)^{\infty} \bullet (\Sigma 0\bar{\Sigma}2)^{\infty}$ is out of the FFZs.

In [4], it had been proved that symmetric periodic orbits cannot undergo period-doubling bifurcations before symmetry breaking in symmetric systems with one parameter. In the map (3) with two parameters A and b, period-doubling bifurcations are also suppressed for symmetric periodic orbits.

Consider a periodic orbit $\Sigma 0\bar{\Sigma}2$. Its period-doubling word is $\Sigma 0\bar{\Sigma}2\Sigma 0\bar{\Sigma}1$. It is clear that

$$\begin{aligned} &\alpha(\bullet(\Sigma 0\bar{\Sigma}1)^{\infty}) < \alpha(\bullet(\Sigma 0\bar{\Sigma}1\Sigma 0\bar{\Sigma}2)^{\infty}) \\ &\beta((\Sigma 0\bar{\Sigma}1)^{\infty}\Sigma 0\bar{\Sigma}2\bullet) < \beta((\Sigma 0\bar{\Sigma}1\Sigma 0\bar{\Sigma}2)^{\infty}\bullet). \end{aligned} \tag{12}$$

Analogously, point $(\Sigma 0\bar{\Sigma}1)^{\infty}\Sigma 0\bar{\Sigma}2 \bullet (\Sigma 0\bar{\Sigma}1)^{\infty}$ is down-left to the point $(\Sigma 0\bar{\Sigma}1\Sigma 0\bar{\Sigma}2)^{\infty} \bullet (\Sigma 0\bar{\Sigma}1\Sigma 0\bar{\Sigma}2)^{\infty}$ in the symbolic plane. Once periodic orbit $\Sigma 0\bar{\Sigma}2\Sigma 0\bar{\Sigma}1$ is allowed, point $\Sigma 0\bar{\Sigma}1 \bullet \Sigma 0\bar{\Sigma}1$ always lies outside the FFZs.

In the case of 1D mapping with only one kneading sequence, equation (12) ensures that the symmetry-breaking orbit $\Sigma 0\bar{\Sigma}1$ is allowed provided that the period-doubling word $\Sigma 0\bar{\Sigma}1\Sigma 0\bar{\Sigma}2$ is admissible. Consequently, we can conclude that the period-doubling bifurcations must be preceded by a bifurcation to asymmetric for the symmetric periodic orbits.

For the 2D mappings, the admissibility of $\Sigma 0\bar{\Sigma}1\Sigma 0\bar{\Sigma}2$ can only ensure that the point $\Sigma 0\bar{\Sigma}1 \bullet \Sigma 0\bar{\Sigma}1$ lies outside the FFZs. There still exists the possibility that the orbit $\Sigma 0\bar{\Sigma}1$ is pruned since there are infinite kneading sequences for 2D mappings. Fortunately, it has been found that the topology of the attractors is almost determined by one kneading sequence completely when the attractor exhibits stable periodic orbits. The possibility to develop period-doubling bifurcations for the symmetric periodic orbits is still highly unlikely.

4. The symmetry-breaking attractors

In this section we discuss the symmetry-breaking attractors. We take the case for $(A, b) = (2.95, 0.25)$ as an example. Figure 5 shows one of the symmetry-breaking attractors. The other symmetry-breaking attractor is symmetric to $(0, 0)$ in the 2D phase space. Figure 6 is the corresponding symbolic plane in which the points represent real trajectories of the attractor in figure 5. It is clear that the symmetry with respect to $(1/2, 1/2)$ is also broken for these points. For these symmetry-breaking attractors, we find the following properties.

(i) All the forward parts of the kneading sequences from C are leading with the following seven letters $K_f = 0102020$. An unstable periodic orbit with length $n < 8$ cannot tell the difference between these kneading sequences. Thus for unstable periodic orbits with length $n < 8$, the grammar for a word allowed or forbidden is completely determined by the

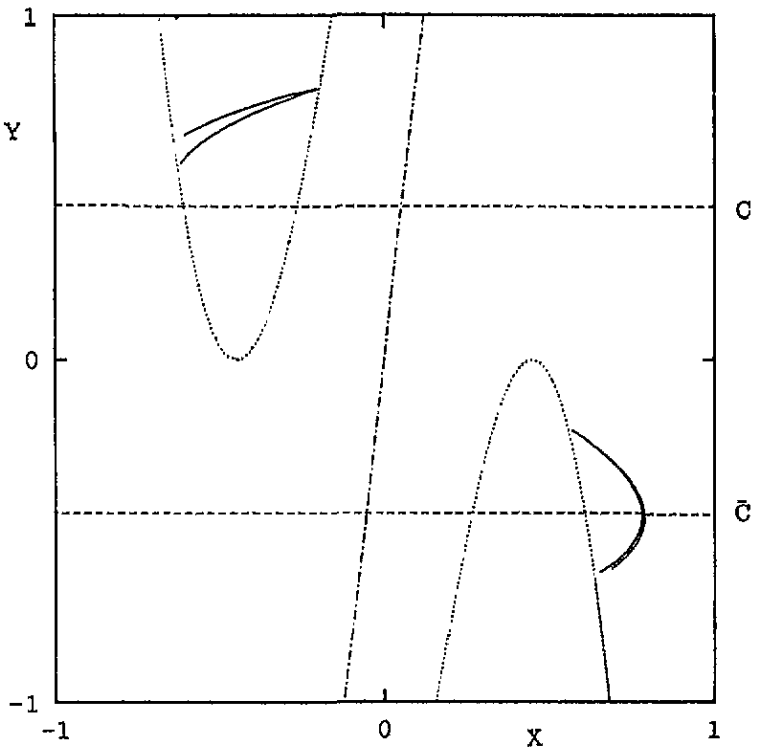

Figure 5. A symmetry-breaking attractor for the antisymmetric cubic map (3) for $(A, b) = (2.95, 0.25)$. The dashed lines are partition lines C and $\bar{C}$. The dash–dotted line and dotted lines are the stable manifolds of the symmetrical period-one orbit 1^∞ and those of period-two orbit $(02)^\infty$, respectively, which are the boundaries between the basins of the two coexisting symmetry-breaking attractors.

sequence K_f, that is, a word $S(x, y)$ corresponds to an unstable periodic orbit of the map (3) for $(A, b) = (2.95, 0.25)$ if and only if it satisfies

$$\alpha(\bar{K}_f) \leqslant \alpha(\sigma^m(\text{Forw}(S(x, y)))) \leqslant \alpha(K_f) \qquad m = 0, 1, 2, \cdots \tag{13}$$

where $\bar{K}_f$ is the conjugate of K_f. This grammar is consistent with that for the 1D antisymmetric cubic map (2) with a kneading sequence K_f. Thus we can say that the topology of the symmetry-breaking attractors of the 2D map (3) is so close to 1D that it can be approximately treated as that of the 1D map with antisymmetric property and, to some degree, two critical points. Numerically we find that all the symmetry-breaking attractors possess this property. It should be noted that unstable periodic orbits in symmetry-breaking attractors with length up to 20 are completely determined by one forward sequence $K_f = 01020101120101010101$ for $(A, b) = (2.93, 0.25)$.

(ii) The two symmetry-breaking attractors are antisymmetric to each other with respect to the original point (0,0). The stable manifolds of the symmetrical period-one orbit 1^∞ (dash–dotted line in figure 5) and those of period-two orbit $(02)^\infty$ (dotted lines) are the boundaries between their attracting basins.

(iii) Symbolically, the trajectories on these two symmetry-breaking attractors share grammar to determine which word is allowed or forbidden. The boundaries are $\bullet 1^\infty$, $\bullet(02)^\infty$, $\bullet 12(02)^\infty$, $\bullet(20)^\infty$ and $\bullet 10(20)^\infty$. All the allowed symbolic sequences $S(x, y)$

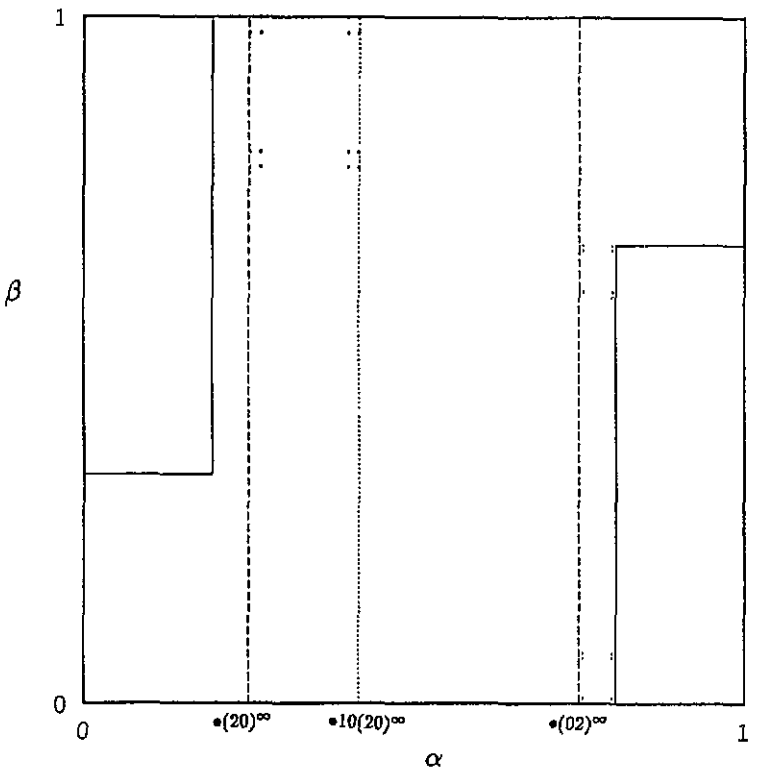

Figure 6. The symbolic plane for the attractor shown in figure 5. Points represent real orbits. The dotted line represents $\alpha = \alpha(\bullet 10(02)^\infty)$ and dashed lines are $\alpha = \alpha(\bullet(02)^\infty)$ and $\alpha = \alpha(\bullet(20)^\infty)$.

belonging to the attractor shown in figure 5 satisfy

$$\alpha(\sigma^m(\text{Forw}(S(x, y)))) > \alpha(\bullet(20)^\infty) \qquad m = 0, \pm 1, \pm 2, \cdots. \tag{14}$$

All the other allowed symbolic sequences satisfy

$$\alpha(\sigma^m(\text{Forw}(S(x, y)))) < \alpha(\bullet(02)^\infty) \qquad m = 0, \pm 1, \pm 2, \cdots \tag{15}$$

belonging to the other symmetry-breaking attractor. We have checked this directly with a Newton procedure up to period 10. This observation is most clearly expressed in the symbolic plane. In figure 6, lines $\alpha = \alpha(\bullet(02)^\infty)$ and $\alpha(\bullet(20)^\infty)$ are also shown as dashed lines. It is clear that all the points lie in the region with $\alpha(\bullet(20)^\infty) < \alpha < \alpha(\bullet 1^\infty) = 0.5$ or $\alpha(\bullet(02)^\infty) < \alpha < \alpha(\bullet 0^\infty) = 1$. We will give a geometric description for this observation in the next section.

5. A geometric description of the symbolic dynamics and the boundaries of basins between coexisting attractors

In 1987, Gu [14] introduced the ideas of most stable manifolds (MSMs) and backward most stable manifolds (BMSMs). An MSM is a submanifold in the basin of an attractor, such that all the points on this submanifold will converge to a single point with the highest possible exponential rate (i.e. the most negative Lyapunov exponent of the attractor). Analogously, a BMSM is also a submanifold. On this submanifold, all the points iterating backward will converge to a single point with the highest possible exponential rate.

The MSMs and BMSMs are extensions of the stable and unstable manifolds of saddles and periodic orbits. If one point of an MSM falls on a stable manifold of a saddle or periodic orbit, this MSM is consistent with this stable manifold. All stable manifolds of saddles and periodic orbits form an invariant subset of MSMs and all unstable manifolds of saddles and periodic orbits form an invariant subset of BMSMs. Consequently, all 'primary' tangencies between stable and unstable manifolds form a subset of the 'primary' tangencies between MSMs and BMSMs.

The MSM and BMSM have a close relationship with symbolic dynamics. Since all the points on an MSM will converge to a single point, all the points sharing a forward sequence must fall on an MSM. Numerically, it has been found that all the points on an MSM share a forward word provided there are no tangency points between them. These tangency points are the images and pre-images of the 'primary' tangency points between MSMs and BMSMs. The sub-space composed of all these points is called a forward foliation (FF). Analogously, all the points sharing a backward sequence form a backward foliation (BF). The MSMs and BMSMs provide a technique to trace the points with the same forward or backward word in the phase space.

In figure 7, two BFs from the unstable symmetrical periodic orbit $(02)^\infty$ and some FFs are shown. The forward words for these FFs are also marked in the figure. It can be checked directly that all the FFs are well ordered on the BFs obeying the ordering rules in equation (5). In fact, all FFs are ordered according to equation (5) on each BF and all BFs are ordered according to equation (7) on each BF. FFs and BFs provide a geometric background on the ordering rules (5) and (7) for forward and backward words in section 2.

This geometric description can be most clearly understood in the following piecewise map:

$$\begin{cases} x_{n+1} = \theta_n + \epsilon_n x_n + b y_n \\ y_{n+1} = x_n \end{cases} \tag{16}$$

where

$$\begin{cases} \theta_n = -\dfrac{c+d}{1-c}\,\mathrm{sgn}(x_n) & \epsilon_n = \dfrac{1+d}{1-c} \qquad c < |x_n| \leqslant 1 \\ \theta_n = 0 & \epsilon_n = -\dfrac{d}{c} \qquad |x_n| \leqslant c. \end{cases}$$

In these equations c, d, b are parameters with all their values between 0 and 1, and $\mathrm{sgn}(x_n)$ denotes the sign of x_n.

$$\mathrm{sgn}(x) = \begin{cases} 1 \\ 0 \\ -1 \end{cases} \quad \text{if} \quad \begin{cases} x > 0 \\ x = 0 \\ x < 0. \end{cases}$$

This piecewise linear map possesses the same antisymmetry as map (3). Note that both map (3) and map (16) share two critical points when b approaches 0. For this piecewise linear map, both BFs and FFs are straight-line segments. We can explicitly define the orderings for forward and backward words by left or right, up or down of the corresponding foliations [15], which gives the ordering rules defined above for map (3).

It is well known that a basin of an attractor is related to stable manifolds. In the case of the symmetry-breaking attractors considered in section 4, the basin boundaries between these two symmetry-breaking attractors are the stable manifolds of the symmetrical period-one orbit 1^∞ and those of the period-two orbit $(02)^\infty$. Symbolically, these basin boundaries correspond to FFs for words $\bullet 1^\infty$, $\bullet(02)^\infty$, $\bullet 12(02)^\infty$, $\bullet(20)^\infty$ and $\bullet 10(20)^\infty$. It can be

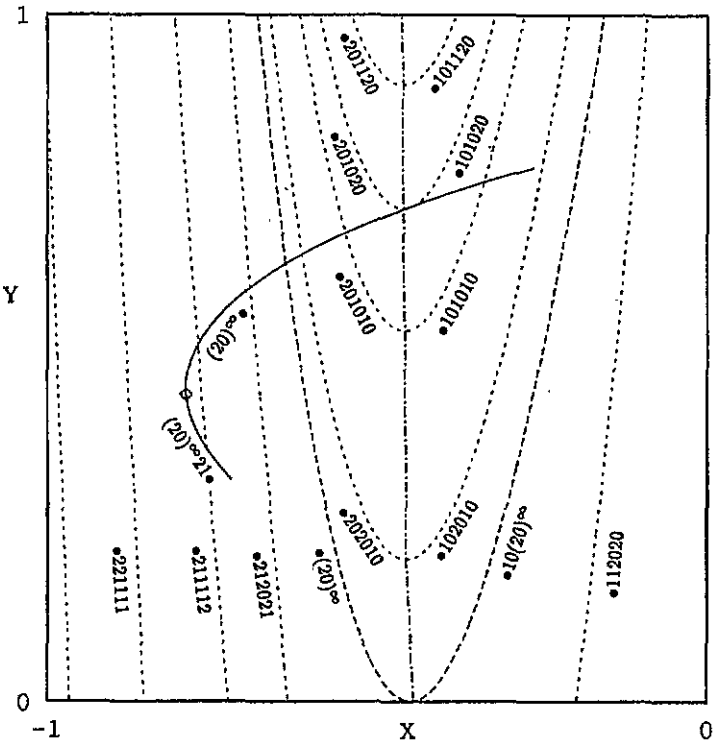

Figure 7. Two BFs and some FFs of the map (3) for $(A, b) = (2.95, 0.25)$. Solid lines are the BFs from the unstable symmetrical periodic orbit $(02)^\infty$. The dashed lines are the FFs which are well ordered on the BFs. The dash–dotted line is the pre-image of the partition line $\bar{C}$ which cuts the MSMs into forward foliations. The diamond is a 'primary' tangency on the BMSM from $(02)^\infty$ which cuts the BMSM into BFs $(20)^\infty\bullet$ and $(20)^\infty 01\bullet$.

checked directly that a point belongs to the basin of the attractor shown in figure 5 if and only if its symbolic sequence $S(x, y)$ satisfies one of the following three conditions,

$$\alpha(\bullet 10(20)^\infty) > \alpha(\text{Forw}(S(x, y)) > \alpha(\bullet(20)^\infty) \tag{17}$$

or

$$\alpha(\bullet 12(02)^\infty) > \alpha(\text{Forw}(S(x, y)) > \alpha(\bullet 1^\infty) \tag{18}$$

or

$$\alpha(\text{Forw}(S(x, y)) > \alpha(\bullet(02)^\infty). \tag{19}$$

Now we consider the symbolic sequences on the attractor in figure 5 explicitly. Since the down part of the attractor in this figure lies in the region right to the FF $\bullet(02)^\infty$, the words $S(x, y)$ of this part satisfy the equation

$$S(x, y) > \bullet(02)^\infty. \tag{20}$$

Likewise, the other part of the symmetry-breaking attractor lies in the region between the FF $\bullet 10(20)^\infty$ and FF $\bullet(20)^\infty$. The words $S(x, y)$ of this part satisfy the equation

$$\bullet 10(20)^\infty > S(x, y) > \bullet(20)^\infty. \tag{21}$$

In figure 6, the dotted line represents the line $\alpha = \bullet 10(20)^\infty$. It is clear that all the points satisfy equations (20) or (21) in the symbolic plane.

6. Conclusions

We have constructed a 2D representation of the symbolic dynamics for the 2D antisymmetric map (3). A symmetrical ternary partition is convenient for this map. Bifurcation in symmetric systems is typically associated with spontaneous symmetry breaking. We discuss the behaviour of the symmetry-breaking periodic orbits, symmetry-breaking bifurcations and symmetry-breaking attractors with this symbolic dynamics. It is still highly unlikely to develop period-doubling bifurcations for the symmetric periodic orbits for this map with two parameters. We have used the forward foliations and backward foliations to understand the symbolic dynamics constructed and the basin boundaries between coexisting attractors.

It should be noted that the discussion in the present work is universal for a large class of dynamical systems with antisymmetry; the map considered in this paper, the Poincaré mappings of the Lorenz equations, the Duffing equations and the 5-mode truncated double-diffusive convection systems are members of this class. Recently, we have succeeded in applying the symbolic dynamics constructed in this paper to the Poincaré mappings of Lorenz equations and the five-mode truncated double-diffusive convection system, determining the topology for these systems. They will be presented elsewhere.

Acknowledgments

The author sincerely thanks Professor Hao Bai-lin for his encouragement during these years, and to Zhao Hong for helpful discussion. This work was partially supported by a grant from CNSF, and by the Computer Center of the ITP which provides us with SUN workstation time.

References

[1] Lorenz E N 1963 *J. Atoms. Sci.* **20** 130
[2] Knobloch E and Weiss N O 1981 *Phys. Lett.* **85A** 127
[3] Ueda Y 1991 *Chaos, Solitons and Fractals* **1** 199
[4] Swift J W and Wiesenfeld K 1984 *Phys. Rev. Lett.* **52** 705
Fang H-P 1993 *Phys. Lett.* **183A** 376
[5] Hénon M 1976 *Commun. Math. Phys.* **50** 65
[6] Hao Bai-lin 1989 *Elementary Symbolic Dynamics and Chaos in Dissipative Systems* (Singapore: World Scientific)
[7] Ding M Z and Hao B L 1988 *Commun. Theor. Phys.* **9** 375
[8] Biham D and Wenzel W 1989 *Phys. Rev. Lett.* **63** 819
[9] Grassberger P, Kantz H 1985 *Phys. Lett.* **113A** 235; 1985 *Physica* **17D** 75
[10] Grassberger P, Kantz H and Moenig U 1989 *J. Phys. A: Math. Gen.* **22** 5217
D'Alessandro G, Grassberger P, Isola S and Politi A 1990 *J. Phys. A: Math. Gen.* **23** 5295
[11] Cvitanovic P, Gunaratne G H and Procaccia I 1988 *Phys. Rev.* A **38** 1503
[12] Flepp L, Holzner R, Brun E, Finardi M and Badii R 1991 *Phys. Rev. Lett.* **67** 2244
Finardi M, Flepp L, Parisi J, Holzner R, Badii R and Brun E 1992 *Phys. Rev. Lett.* **68** 2989
[13] Auerbach D, Cvitanovic P, Echmann J P, Gunaratne G H and Procaccia I 1987 *Phys. Rev. Lett.* **58** 2387
[14] Gu Y 1987 *Phys. Lett.* **124A** 340
[15] Fang H-P 1994 Symbolic dynamics for a piecewise linear 2D antisymmetric map (in preparation)